Journal of Non-Crystalline Solids 619 (2023) 122582

Contents lists available at ScienceDirect

Journal of Non-Crystalline Solids

journal homepage: www.elsevier.com/locate/jnoncrysol

Improved wear resistance of metallic glacier glass

Zhe Chen [a], Fei Sun [a], Wenxue Wang [a], Jianyu Chen [a], Shuai Ren [a,b,*], Wenqing Ruan [a,b,*], Jiang Ma [a,b,*]

[a] Guangdong Key Laboratory of Electromagnetic Control and Intelligent Robots, Shenzhen University, Shenzhen 518060, China

[b] Shenzhen Key Laboratory of High Performance Nontraditional Manufacturing, College of Mechatronics and Control Engineering, Shenzhen University, Shenzhen 518060, China

ARTICLE INFO

Keywords:
Wear resistance
Metallic glasses
Metallic glacial glasses
Liquid-liquid transition
Dynamic relaxations

ABSTRACT

Metallic glasses (MGs) have garnered significant attention due to their excellent properties, like high wear resistance, making them highly promising for a wide range of engineering applications. However, it is of significance to further increase the wear resistance of MGs, which has rarely been studied. Here we present a remarkable enhancement of wear resistance when some MGs undergo a liquid-liquid transition to form a new metallic glacial glass (MGG) state. Within an identical composition of $La_{65}Ni_{20}Al_{15}$, the wear resistance of the MGG exhibits a notable superiority of 104% compared to the as-cast MG, and an even more remarkable advantage of 349% compared to its crystalline counterpart. The excellent wear resistance of the MGG is attributed to its ultrastable nature in energy confirmed by dynamic relaxation changes. This work not only offers a unique perspective on MGs, but also provides an effective technique for developing wear-resistant materials.

1. Introduction

Metallic glasses (MGs) are unique materials that are synthesized by rapid cooling of molten liquids to avoid crystallization [1,2]. Due to the absence of long-range atomic packing ordering and conventional defects like dislocations and grain boundaries, MGs exhibit remarkable properties, such as large elastic limit, high yield strength and high hardness [3–6]. These properties render them suitable for various applications such as micro-gears and bearing structures [3,4].

On the other hand, friction between components is an inevitable occurrence in engineering applications and may result in excessive wear, which is one of the main causes of equipment failure. The conventional wear-resistant materials are generally crystalline materials, including tungsten carbide [7,8], silicon carbide [9,10], and diamond [11,12]. Recently, there has been extensive research focused on wear resistance in amorphous alloys (namely MGs) [13–17], which have been found to exhibit excellent capability to resist wear in a wide temperature range, particularly at elevated temperatures reaching 750 °C [14].

It is well known that the properties of MGs strongly depend on their energy state which can be tuned by aging [15,17–19]. Aging makes the MGs undergo structural relaxation, which is manifested by the reduction of enthalpy below the glass transition temperature (T_g). The mechanical and tribological properties of MGs vary with their energy state after structural relaxation accordingly [15,20,21]. Jin et al. [22] found that the heat treatment of $Zr_{42}Ti_{15.5}Cu_{14.5}Ni_{3.5}Be_{24.5}$ MG at 0.83 T_g can reduce its wear volume by approximately 34%. Moreover, it has been reported that the wear rate of the relaxed $Cu_{60}Zr_{30}Ti_{10}$ MG is 65% lower than that of the as-cast counterpart [17]. Another work has also shown that the relaxed MG of $Zr_{60}Cu_{10}Al_{15}Ni_{15}$ exhibited the best wear resistance compared to the as-cast MG and crystalline states [18]. Pre-heating during the wear process or frictional heating has also been shown to cause structural relaxation in MGs and alter their surface chemistry [17]. Consequently, the wear resistance of MGs seems to increase with the reduction of their energy level with aging.

In recent years, liquid-liquid phase transitions have been discovered in some specific amorphous systems, which lead to a new glass state [23–27]. In the study of Shen et al., a liquid-liquid transition is found in Rare-earth-based metallic glasses, and a new metallic glass emerges after the liquid-liquid transition [23]. This new glass phase is called metallic glacier glass (MGG), which possesses a higher T_g and a less enthalpy change (i.e., smaller area of the exothermic peaks during heating) than those of the as-cast counterpart. Therefore, the MGG is considered to be a thermodynamically ultrastable state [23,26,27], with an energy level much lower than that of the samples aged below T_g. As a consequence, it invites an important and intriguing question: how are properties of the MGG as an ultrastable glassy state?

* Corresponding authors at: Guangdong Key Laboratory of Electromagnetic Control and Intelligent Robots, Shenzhen University, Shenzhen 518060, China.
E-mail addresses: shuai.ren@szu.edu.cn (S. Ren), ruanwq@szu.edu.cn (W. Ruan), majiang@szu.edu.cn (J. Ma).

https://doi.org/10.1016/j.jnoncrysol.2023.122582
Received 11 July 2023; Received in revised form 14 August 2023; Accepted 16 August 2023
Available online 23 August 2023
0022-3093/

In this work, we report a remarkable improvement in wear resistance for the MGG, exhibiting a significant enhancement of 104% compared to the same composition in its as-cast state and an impressive enhancement of 349% compared to the same composition in its crystalline state. The hardness of the MGG only increases slightly compared to the as-cast state. DMA tests showed that both α-relaxation and β-relaxation in the MGG shifted to higher temperatures, and the activation energy of β-relaxation increases. It indicates that the MGG locates at a much lower energy state than the as-cast counterpart, which contributes to the remarkable enhancement in wear resistance. This finding provides a direction for exploring higher wear-resistant materials and a better understanding of the properties of the MGG.

2. Experiments

$La_{65}Ni_{20}Al_{15}$ (at.%, abbreviated as La65 hereafter) alloy was synthesized by arc melting pure La (99.9at.%), Ni (99.999at.%), and Al (99.999at.%) in a high-purity argon atmosphere. A titanium ingot was used for the melting process at high temperature to prevent oxidation. To ensure the uniform composition of the molten alloy, each ingot was melted 8–10 times, and then cast into a plate with a width of 20 mm and a thickness of 2 mm using a water-cooled copper crucible. These La-based BMGs were cut into 10 mm diameter disks by using low-speed wire electrical discharge machining (WEDM; SODICK AP250L).

The phase structure of the samples was examined using X-ray diffraction of CuKα radiation (XRD, Rigaku MiniFlex 600), and a scan rate of 2 rad/min was used. The glass properties of the samples were determined using differential scanning calorimetry (DSC, Perkin Elmer DSC-8000) at a heating rate of 20 K/min. The micromorphology and elemental distribution of the samples were characterized using transmission electron microscopy (TEM, FEI Titan Cubed Themis G2 300) and (EDS). The TEM samples were prepared on a FEI Scios SEM/FIB dual beam system.

Dry sliding wear tests were performed on the top surface of BMG samples under air atmosphere using a ball-and-disk wear machine (Rtec MFT-5000, USA). A commercial zirconium dioxide (ZrO_2) balls (9.5 mm diameter) with a hardness of ~14 GPa were selected as the corresponding components. A fixed sliding speed of 200 r min^{-1}, a total sliding time of 30 min, and a load of 10 N were applied to all wear tests. The 3D morphology of the wear trajectory and the amount of wear were evaluated using a white light interferometer (Bruker ContourGT-X 3D). The 3D morphology and wear volume of the wear trajectory were evaluated using a white light interferometer (Bruker ContourGT-X 3D).

The modulus of the BMG samples was tested by using a nanoindenter (TI750 Hysitron Ltd.). Sixteen points per sample were tested to ensure the reliability of the data. The maximum load was 5 mN. The relaxation features were performed by the dynamic mechanical analyzer (DMA, TA DMA-Q850), where frequencies of 0.2 Hz, 0.4 Hz, 1 Hz, 2 Hz, 4 Hz, 10 Hz, and 20 Hz were used.

3. Results

Fig. 1(a) shows the DSC curves of the as-cast MG and MGG in La65. The T_g of the as-cast sample is determined around 438 K, and its first exothermic peak temperature (T_p) is around 453 K. The MGG is obtained by heating to 473 K at a rate of 10 K/min, followed by cooling down immediately at a rate of 100 K/min. The heat treatment temperature is above the T_p of the as-cast one, as shown by the red arrow. It is clear that the T_g of the MGG increases, while the first exothermic peak disappears.

The X-ray diffraction (XRD) patterns of three samples are shown in Fig. 1(b). The black pattern corresponds to the as-cast MG, which exhibits a distinct halo characteristic of the amorphous structure. The red pattern corresponds to the XRD pattern of the MGG in which the amorphous halo peaks still retain. More interestingly, the second halo peak is enhanced, which is a typical structure characteristic of the MGG [23,27]. The blue pattern shows the XRD data of the crystalline state after annealing at 673 K for 10 min, and sharp peaks are observed. High-resolution electron micrographs and the corresponding diffraction pattern images of the as-cast MG and MGG are shown in Figs. 1(c,d), respectively. The characteristic halos of amorphous phase are observed

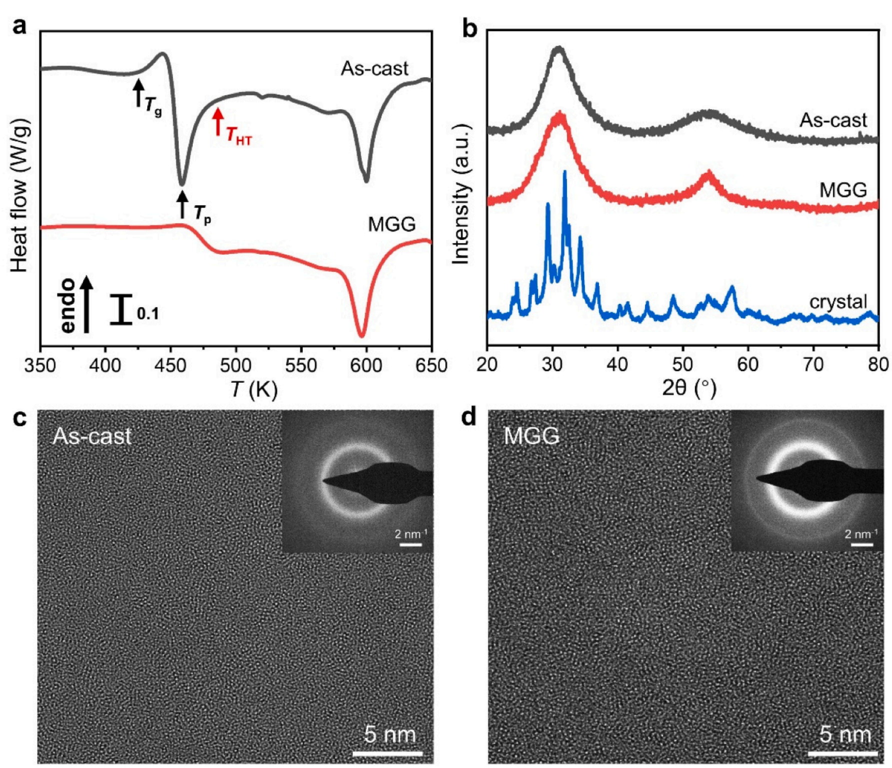

Fig. 1. DSC curves and structure of as-cast MG, MGG and crystalline samples. (a) DSC curves corresponding to as-cast MG and MGG. (b) XRD patterns of the three samples. (c, d) HRTEM images of (c) as-cast MG and (d) MGG with the corresponding SAED images.

and no crystalline structure is found in both of them. It reveals an amorphous structure down to the atomic level. Thus, it can be confirmed that the MGG remains an amorphous state.

The wear behaviors of the three states, including as-cast MG, MGG, and crystalline phase, are shown in Fig. 2(a, d, g) which display the relationship between coefficient of friction (COF) and time for the three states. In the early stages of wear, there is an abrupt increase in the COF, subsequently followed by a gradual decrease or stabilization, which is commonly known as "running-in" related to the roughness of the contacting surfaces [14,28]. It is noted that the MGG sample undergoes a longer "running-in" period, indicating higher wear resistance than the other two samples. Fig. 2(b, e, h) present a comparative analysis of the three-dimensional profiles of the wear tracks for the three samples. It is found that the MGG sample demonstrates the least severe wear, whereas the crystalline sample exhibits the most severe wear. Based on the cross-sectional profiles shown in Fig. 2(c, f, i), the depths of the wear tracks are 50.908 μm (d_{Max1}) for the as-cast MG, 32.606 μm (d_{Max2}) for the MGG, and 97.034 μm (d_{Max3}) for the crystalline sample, respectively. The integrated wear track areas for the as-cast MG, MGG and crystalline samples are 45,498 μm^2 (S_1), 22,256 μm^2 (S_2), and 99,879 μm^2 (S_3), respectively. The wear rate ω is derived from the volume-loss equation [14] as follows: $\omega = V_{loss} /(L*P)$, Where V_{loss} is the total volume lost (mm^3), L is the total wear distance (m) calculated from the wear time (min), wear speed (rpm) and wear radius (mm), and P is the applied load (N). The wear rates are calculated as: 7.583×10^{-3}mm^{-3}N^{-1}m^{-1} for the as-cast MG, 3.079×10^{-3}mm^{-3}N^{-1}m^{-1} for the MGG, 16.65×10^{-3}mm^{-3}N^{-1}m^{-1} for the crystalline phase.

In order to investigate the wear mechanism of the above samples, we examined the wear marks using SEM and EDS. In Fig. 3(a, d, g), the presence of wear trace is observed for the three states. The occurrence of delamination is found in Fig. 3(a, d), which can be attributed to plastic deformation in amorphous alloys. It is obvious that the wear trace width of the MGG sample is the narrowest, about 1.119 mm. This result serves as further evidence substantiating the enhanced wear resistance of the MGG sample.

A detailed analysis of the wear mechanism of the as-cast MG is depicted in Fig. 3(b, c), providing a clear observation of the formation of grooves, delamination, and debris. These characteristics have been reported previously in the wear surfaces of bulk metallic glasses (BMG) [29–32]. Subsequently, elemental analysis was conducted on these wear areas and summarized in Table 1. The distribution of elements in the non-wear region (P_1), delaminated region (P_2, P_4) and peeling region (P_3) in Fig. 3(b, c) is shown in Table 1. The oxygen content in the non-wear region, delaminated region and peeling region are 5.6% (P_1), 35.2% (P_2), 48.1% (P_3) and 36.5% (P_4), respectively. Based on these results, we can know that the wear mechanism of as-cast MG is a combination of oxidative wear, adhesive wear and abrasive wear.

Microcracks, peeling and delamination are clearly visible in Fig. 3(e, f) of the MGG, indicating severe plastic deformation of the MGG in the direction of wear. Element distributions in the non-worn region (P_5), peeling regions (P_6, P_8) and delaminated regions (P_7, P_9) were detected. As shown in Table 1, the oxygen contents in the non-worn, peeling and delaminated regions are 8.8% (P_5), 49.6% (P_6), 31.0% (P_7), 52.9% (P_8) and 35.4% (P_9). These results are similar to those previously reported by Bhatt et al. for the worn surface of a relaxed sample [17]. Based on these results, it can be concluded that the wear mechanism of the MGG sample is a combination of oxidative wear, adhesive wear and fatigue wear.

The grooves and debris can be clearly seen in Fig. 3(h, i)

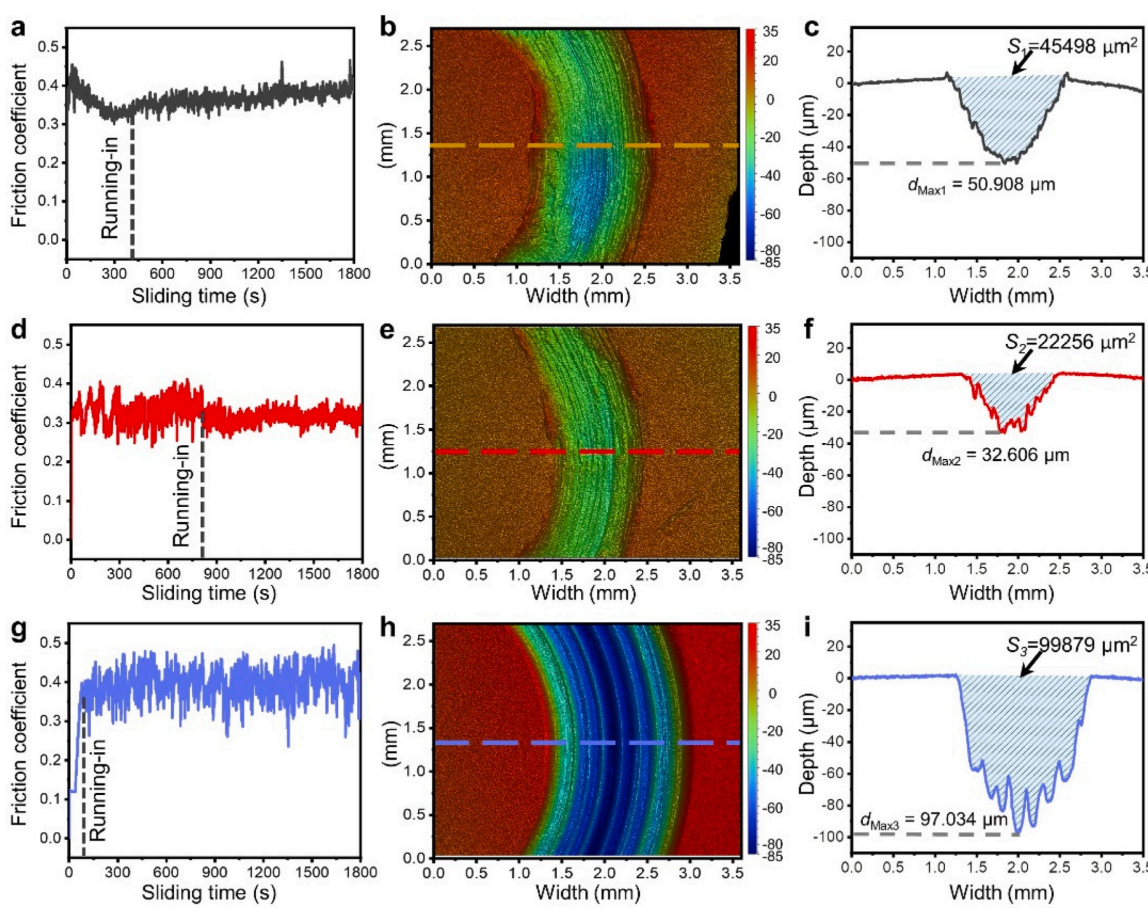

Fig. 2. Characterization of frictional wear of three samples. (a, d, g,) COF versus time for (a) as-cast MG, (d) MGG, and (g) crystalline state. (b, e, h) Wear morphology of (b) as-cast MG, (e) MGG, and (g) crystalline state. (c, f, i) Cross-sectional profile of (c) as-cast MG, (f) MGG, and (i) crystalline state wear marks.

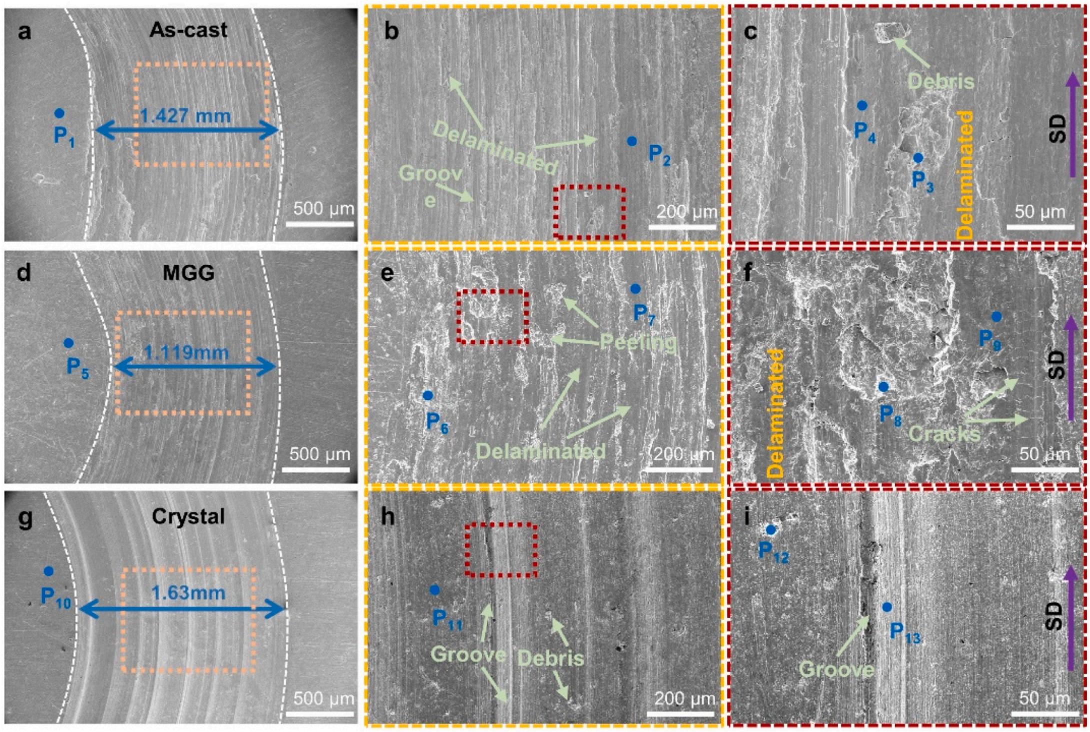

Fig. 3. Wear patterns of three samples. (a-c) Wear morphology and elemental analysis of as-cast BMG. (d-f) Wear morphology and elemental analysis of MGG. (g–i) Wear morphology and elemental analysis of crystalline phase. Points are labelled for elemental analysis.

Table 1
The statistics of elemental oxygen content in different regions.

Point No.	Element Content (at.%)			
	La	Ni	Al	O
P_1	62.5	17.2	14.7	5.6
P_2	46.3	11.6	6.9	35.2
P_3	36.5	8.5	6.9	48.1
P_4	47.9	11.7	3.9	36.5
P_5	65.2	15.8	10.2	8.8
P_6	35.0	7.5	7.9	49.6
P_7	46.1	14.1	8.9	31.0
P_8	31.0	8.5	7.5	52.9
P_9	45.2	10.9	8.5	35.4
P_{10}	63.3	13.6	13.8	9.3
P_{11}	44.4	10.5	9.0	36.1
P_{12}	26.0	6.8	5.7	61.5
P_{13}	35.0	7.2	7.0	50.8

corresponding to the crystalline phase. The distribution of elements in the non-wear area (P_{10}), debris area (P_{12}), and grooves (P_{11}, P_{13}) were examined. The results are shown in Table 1. Oxygen content in the debris area up to 61.5% and the grooves area also has a high oxygen content. Based on these results, it can be concluded that the wear mechanisms of the crystallized alloy are abrasive wear and oxidative wear.

4. Discussion

The COF and wear rate of three different states are summarized in Fig. 4(a). A compelling demonstration has been provided, showcasing that the MGG exhibits low friction coefficient and low wear rate. Previous literature has reported a negative correlation between hardness and wear rate [17,18]. Thus, we also tested the material intrinsic mechanical properties, i.e., hardness and modulus. The hardness results of the tests using a microhardness tester are shown in Fig. 4(b), where 40 points are taken for each sample to minimize errors. It can be clearly seen that the microhardness of MGG is the highest, while the as-cast MG is the lowest. Nanoindentation patterns are measured using nanoindentation with a peak load of 5 mN and the corresponding load-displacement curves are shown in Fig. 4(c). Sixteen points were taken for each sample and the results are shown in Fig. 4(d), where the modulus results follow the same trend as the microhardness results. It has been reported that during the heat treatment, a denser random stacking structure is obtained due to the annihilation of the free volume, leading to a limitation of shear band motion in the relaxed amorphous alloy and an increase in hardness [17,33,34]. This coincides with our experimental results.

Although the microhardness and nanoindentation values of the crystalline alloy are higher than those of the as-cast MG (Fig. 4(b, d)), the wear capability of the crystal is lower than that of the as-cast MG. This result is due to the different wear mechanisms in MGs and crystals [35]. The main mode of wear for crystalline materials is abrasive wear. Crystalline materials undergo plastic deformation through dislocation movements [36,37]. In contrast to pure metals or conventional alloys, metallic glasses are devoid of dislocations. The wear mechanism of metallic glasses involves inhomogeneous shear. The inhomogeneous plastic flow is evident through the formation of local shear bands [15, 38]. This shear instability in MGs is due to softening and therefore high deformation of the region appears near the shear zone [17]. Previous studies [33,34] revealed inhomogeneous shear bands within the wear trajectory of metallic glasses. Consistent with the wear profile of this work.

The above results show that the hardness of the MGG becomes slightly higher than that of the as-cast sample by 8.5%, but the wear resistance remarkably increases to 104%. Therefore, the slight hardness increase is not the main reason of the remarkable enhancement in wear resistance. To figure out the key reason, we performed further study on the relaxation behaviors of the as-cast MG and MGG.

Fig. 5(a) shows the loss modulus curves of as-cast MG and MGG. Two relaxation peaks can be observed in their curves, the low temperature peak is the β-relaxation peak and the high temperature peak is the

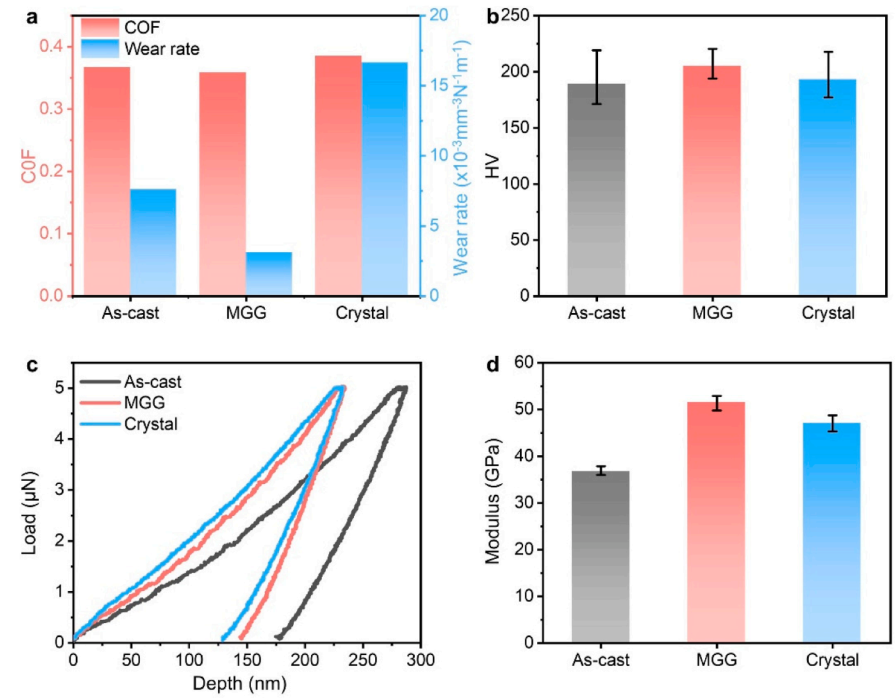

Fig. 4. Summarizes the COF, wear rate, hardness and modulus of the material for the three samples. (a) Summary of the friction coefficient and wear rate of the three samples. (b) Microhardness results for the three samples. (c) Nanoindentation curves for the three samples. (d) Modulus statistics for the three samples.

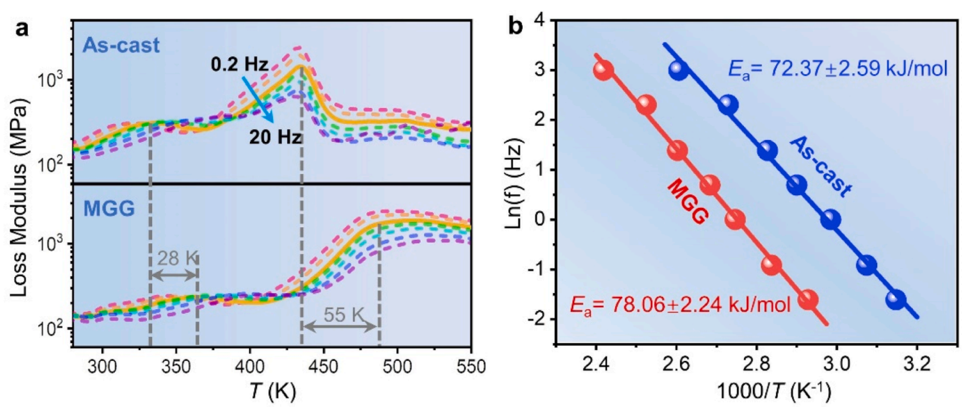

Fig. 5. Dynamic features of the as-cast MG and MGG. (a) Loss modulus curves of the MG and MGG. The solid curves at 1 Hz are used as references for determining peak temperature changes. (b) Arrhenius fitting of peak temperature and frequency of β-relaxation for both the MG and MGG. According to the Arrhenius relation, the activation energies are yielded.

α-relaxation peak. The results show that the α-relaxation peak temperature and the β-relaxation peak temperature of the MGG are higher than those of the as-cast state. The peak temperature rise of the β-peak is around 28 K and the rise of the α-peak is up to 55 K. These peak temperature rises are consistent with the T_g change in DSC results in Fig. 1 (a) and indicate that the MGG is thermodynamically more stable than the as-cast state. Fig. 5(b) shows the frequency (f) of the β-peaks versus peak temperature (T_β) in the as-cast MG and MGG, which can be fitted by the Arrhenius relation,

$$f = f_0 * \exp\left(-E_a / RT_\beta\right), \tag{1}$$

where f_0 is the prefactor, E_a is the β-relaxation activation energy, and R is the gas constant. The E_a of as-cast MG and MGG are yielded to be 72.37 ±2.59 kJ/mol and 78.06±2.24 kJ/mol, respectively. The higher E_a indicates the MGG locates at lower energy states, so it is more difficult to activate the β-relaxation of the MGG. From the view of microstructure, the MGG has been reported to possess a denser random stacking structure [17], indicating a substantial annihilation of the free volume when the as-cast MG transforms into the MGG. As a consequence, the much lower energy state of the MGG leads to a much more difficulty to generate shear band motion, and thus the MGG exhibits much better wear resistance than that of the as-cast MG.

5. Conclusions

In this work, we report a remarkable improvement of wear resistance in the MGG. It exhibits a significant enhancement of 104% compared to the same composition in its as-cast MG and an impressive enhancement of 349% compared to the same composition in its crystalline state. DMA tests showed that both α-relaxation and β-relaxation in the MGG shifted to higher temperatures, and the activation energy of β-relaxation increases. It indicates the MGG locates at a much lower energy state than the as-cast counterpart, which contributes to the remarkable enhancement in wear resistance. This work provides a promising route to improve the wear performance of metallic glasses and offers a new perspective on understanding liquid-liquid phase transitions.

CRediT authorship contribution statement

Zhe Chen: Conceptualization, Formal analysis, Investigation, Project administration, Software, Supervision, Writing – original draft, Writing – review & editing. **Fei Sun:** Conceptualization, Formal analysis, Investigation, Project administration, Software, Supervision, Writing – original draft, Writing – review & editing. **Wenxue Wang:** Conceptualization, Formal analysis, Investigation, Project administration, Software, Supervision, Writing – original draft, Writing – review & editing. **Jianyu Chen:** Conceptualization, Formal analysis, Investigation, Project administration, Software, Supervision, Writing – original draft, Writing – review & editing. **Shuai Ren:** Conceptualization, Formal analysis, Investigation, Project administration, Software, Supervision, Writing – original draft, Writing – review & editing. **Wenqing Ruan:** Conceptualization, Formal analysis, Investigation, Project administration, Software, Supervision, Writing – original draft, Writing – review & editing. **Jiang Ma:** Conceptualization, Formal analysis, Investigation, Project administration, Software, Supervision, Writing – original draft, Writing – review & editing.

Declaration of Competing Interest

The authors declare that they have no known competing financial interests or personal relationships that could have appeared to influence the work reported in this paper.

Data availability

The data that has been used is confidential.

Acknowledgment

The work was financially supported by the Key Basic and Applied Research Program of Guangdong Province, China (Grant No. 2019B030302010), the NSF of China (Grant No. 52122105, 51971150, 51901243), the Science and Technology Innovation Commission Shenzhen (Grants No. RCJC20221008092730037, 20220804091920001) and the National Key Research and Development Program of China (Grant No. 2018YFA0703605). The authors also thank the assistance on microscope observation received from the Electron Microscope Center of Shenzhen University.

References

[1] A.L. Greer, Metallic glasses on the threshold, Mater. Today 12 (2009) 14–22.
[2] M.D. Ediger, C.A. Angell, S.R. Nagel, Supercooled liquids and glasses, J. Phys. Chem. A 100 (1996) 13200–13212.
[3] W.H. Wang, C. Dong, C.H. Shek, Bulk metallic glasses, Mat. Sci. End. R 44 (2004) 45–89.
[4] W.H. Wang, Bulk metallic glasses with functional physical properties, Adv. Mater. 21 (2009) 4524–4544.
[5] L. Tian, Y.Q. Cheng, Z.W. Shan, J. Li, C.C. Wang, X.D. Han, J. Sun, E. Ma, Approaching the ideal elastic limit of metallic glasses, Nat. Commun. 3 (2012) 609.
[6] D.C. Hofmann, J.Y. Suh, A. Wiest, G. Duan, M.L. Lind, M.D. Demetriou, W. L. Johnson, Designing metallic glass matrix composites with high toughness and tensile ductility, Nature 451 (2008) 1085–1089.
[7] J.A. Arsecularatne, L.C. Zhang, C. Montross, Wear and tool life of tungsten carbide, PCBN and PCD cutting tools, Int. J. Mach. Tools Manuf. 46 (2006) 482–491.
[8] K. Van Acker, D. Vanhoyweghen, R. Persoons, J. Vangrunderbeek, Influence of tungsten carbide particle size and distribution on the wear resistance of laser clad WC/Ni coatings, Wear 258 (2005) 194–202.
[9] J. Takadoum, Z. Zsiga, C. Roquescarmes, Wear mechanism of silicon-carbide - new observations, Wear 174 (1994) 239–242.
[10] X. Dong, S. Jahanmir, L.K. Ives, Wear transition diagram for silicon carbide, Tribol. Int. 28 (1995) 559–572.
[11] Y. Liu, A. Erdemir, E.I. Meletis, A study of the wear mechanism of diamond-like carbon films, Surf. Coat. Tech. 82 (1996) 48–56.
[12] L. Pastewka, S. Moser, P. Gumbsch, M. Moseler, Anisotropic mechanical amorphization drives wear in diamond, Nat. Mater. 10 (2011) 34–38.
[13] Q. Zhou, D. Luo, D. Hua, W. Ye, S. Li, Q. Zou, Z. Chen, H. Wang, Design and characterization of metallic glass/graphene multilayer with excellent nanowear properties, Friction 10 (2022) 1913–1926.
[14] F. Sun, S.T. Deng, J.A. Fu, J.H. Zhu, D.D. Liang, P.F. Wang, H. Zhao, F. Gong, J. Ma, Y.H. Liu, J. Shen, Superior high-temperature wear resistance of an Ir-Ta-Ni-Nb bulk metallic glass, J. Mater. Sci. Technol. 158 (2023) 121–132.
[15] A. Concustell, G. Alcala, S. Mato, T.G. Woodcock, A. Gebert, J. Eckert, M.D. Baro, Effect of relaxation and primary nanocrystallization on the mechanical properties of Cu60Zr22Ti18 bulk metallic glass, Intermetallics 13 (2005) 1214–1219.
[16] G.Q. Zhang, X.J. Li, M. Shao, L.N. Wang, J.L. Yang, L.P. Gao, L.Y. Chen, C.X. Liu, Wear behavior of a series of Zr-based bulk metallic glasses, Mater. Sci. Eng. A 475 (2008) 124–127.
[17] J. Bhatt, S. Kumar, C. Dong, B.S. Murty, Tribological behaviour of Cu60Zr30Ti10 bulk metallic glass, Mater. Sci. Eng. A Struct. 458 (2007) 290–294.
[18] R. Salehan, H.R. Shahverdi, R. Miresmaeili, Effects of annealing on the tribological behavior of Zr60Cu10Al15Ni15 bulk metallic glass, J. Non Cryst. Solids 517 (2019) 127–136.
[19] X.Q. Fu, C.L. Li, X.C. Li, C.Y. Li, Y.C. Zhao, Y.T. Ding, S.Z. Kou, Effect of heat treatment on the frictional wear properties of Zr-based amorphous alloy, J. Mater. Eng. Perform. (2023), https://doi.org/10.1007/s11665-023-08191-y.
[20] Y. Yue, C.A. Angell, Clarifying the glass-transition behaviour of water by comparison with hyperquenched inorganic glasses, Nature 427 (2004) 717–720.
[21] Y. Zhao, B. Shang, B. Zhang, X. Tong, H. Ke, H. Bai, W.H. Wang, Ultrastable metallic glass by room temperature aging, Sci. Adv. 8 (2022) eabn3623.
[22] H.W. Jin, R. Ayer, J.Y. Koo, R. Raghavan, U. Ramamurty, Reciprocating wear mechanisms in a Zr-based bulk metallic glass, J. Mater. Res. 22 (2007) 264–273.
[23] J. Shen, Z. Lu, J.Q. Wang, S. Lan, F. Zhang, A. Hirata, M.W. Chen, X.L. Wang, P. Wen, Y.H. Sun, H.Y. Bai, W.H. Wang, Metallic glacial glass formation by a first-order liquid-liquid transition, J. Phys. Chem. Lett. 11 (2020) 6718–6723.
[24] Y.G. So, S. Sato, K. Edagawa, R. Tamura, Internal friction of an Al–Cu–Fe icosahedral quasicrystal and its crystal approximant, Philos. Mag. 91 (2010) 2820–2827.
[25] G. Li, Y.Y. Wang, P.K. Liaw, Y.C. Li, R.P. Liu, Electronic structure inheritance and pressure-induced polyamorphism in lanthanide-based metallic glasses, Phys. Rev. Lett. 109 (2012), 125501.
[26] H.W. Sheng, H.Z. Liu, Y.Q. Cheng, J. Wen, P.L. Lee, W.K. Luo, S.D. Shastri, E. Ma, Polyamorphism in a metallic glass, Nat. Mater. 6 (2007) 192–197.
[27] S. Lan, Y. Ren, X.Y. Wei, B. Wang, E.P. Gilbert, T. Shibayama, S. Watanabe, M. Ohnuma, X.L. Wang, Hidden amorphous phase and reentrant supercooled liquid in Pd-Ni-P metallic glasses, Nat. Commun. 8 (2017) 14679.
[28] Y. Jiang, Z.M. Xie, J.F. Yang, Q.F. Fang, High-temperature tribological behavior of tungsten, Int. J. Refract. Met. Hard Mater. 84 (2019) 104992.
[29] M.L. Rahaman, L.C. Zhang, Size effect on friction and wear mechanisms of bulk metallic glass, Wear 376 (2017) 1522–1527.
[30] T.S. Eyre, Wear characteristics of metals, Tribol. Int. 9 (1976) 203–212.
[31] H. Wu, I. Baker, Y. Liu, X.L. Wu, Dry sliding tribological behavior of Zr-based bulk metallic glass, Trans. Nonferrous Met. Soc. China 22 (2012) 585–589.
[32] M.L. Rahaman, L.C. Zhang, H.H. Ruan, Understanding the friction and wear mechanisms of bulk metallic glass under contact sliding, Wear 304 (2013) 43–48.
[33] U.S. Kishore, N. Chandran, K. Chattopadhyay, On the wear mechanism of iron and nickel based transition-metal metalloid metallic glasses, Acta Metall. Mater. 35 (1987) 1463–1473.
[34] K. Miyoshi, D.H. Buckley, Microstructure and surface-chemistry of amorphous-alloys important to their friction and wear behavior, Wear 110 (1986) 295–313.
[35] Y. Ren, Z. Huang, Y. Wang, Q. Zhou, T. Yang, Q. Li, Q. Jia, H. Wang, Friction-induced rapid amorphization in a wear-resistant (CoCrNi)88Mo12 dual-phase medium-entropy alloy at cryogenic temperature, Compos. B Eng. 263 (2023) 110833.
[36] W. Wang, D. Hua, D. Luo, Q. Zhou, S. Li, J. Shi, H. Wang, Molecular dynamics simulation of deformation mechanism of CoCrNi medium entropy alloy during nanoscratching, Comput. Mater. Sci. 203 (2022) 111085.
[37] Y. Du, X. Pei, Z. Tang, F. Zhang, Q. Zhou, H. Wang, W. Liu, Mechanical and tribological performance of CoCrNiHf eutectic medium-entropy alloys, J. Mater. Sci. Technol. 90 (2021) 194–204.
[38] A.L. Greer, Y.Q. Cheng, E. Ma, Shear bands in metallic glasses, Mater. Sci. Eng. R Rep. 74 (2013) 71–132.